Examining DNA Structures with In-droplet Hydrogen/Deuterium Exchange Mass Spectrometry

Kushani Attanayake, Sultan Mahmud*, Chandrima Banerjee, Daud Sharif, Mohammad Rahman, Sandra Majuta, Anthony DeBastiani, Mst Nigar Sultana, Samira Hajian Foroushani, Chong Li, Peng Li, Stephen J. Valentine*

C. Eugene Bennett Department of Chemistry, West Virginia University, Morgantown, WV, USA.

Correspondence should be addressed to Stephen Valentine (stephen.valentine@mail.wvu.edu)

*Authors contributed equally to this work.

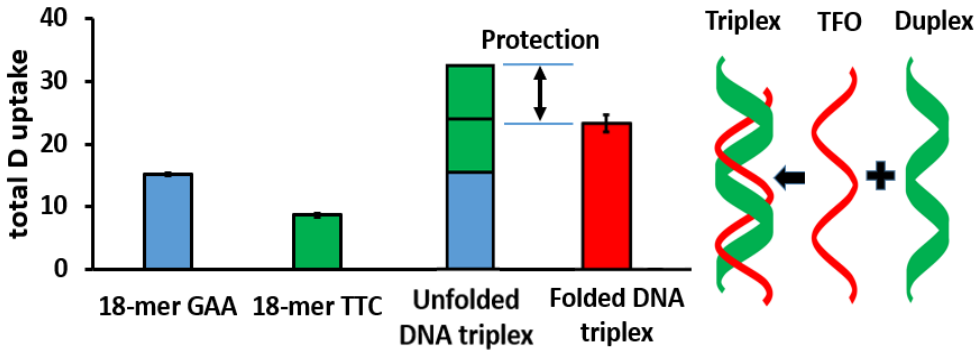

Abstract

Capillary vibrating sharp-edge spray ionization (cVSSI) combined with hydrogen/deuterium exchange-mass spectrometry (HDX-MS) has been utilized to characterize different solution-phase DNA conformers including DNA G-quadruplex topologies as well as triplex DNA and duplex DNA. In general, G-quadruplex DNA shows a wide range of protection of hydrogens extending from ~12% to ~21% deuterium incorporation. Additionally, parallel, antiparallel, and hybrid G-quadruplex topologies exhibit slight differences in deuterium uptake levels. Notably, the exchange levels for hybrid sub topologies of G-quadruplex DNA (Hybrid 1 and Hybrid 2) are significantly different although the DNA sequences are highly comparable. For the quadruplex-forming sequences, correlation analysis suggests protection of base hydrogens involved in tetrad hydrogen bonding. For duplex DNA ~19% deuterium incorporation is observed while only ~16% is observed for triplex DNA. This increased protection of hydrogens may be due to the added backbone scaffolding and Hoogsteen base pairing of the latter species. These experiments lay the groundwork for future studies aimed at determining the structural source of this protection as well as the applicability of the approach for ascertaining different oligonucleotide folds and co-existing conformations.

Introduction

After the introduction of soft ionization techniques, hydrogen/deuterium exchange-mass spectrometry (HDX-MS) emerged relatively early as a powerful analytical tool that can provide insight into conformations, conformational heterogeneity, and dynamics of higher-order protein structure.[1-8] Early structural studies employing isotopic exchange experiments utilized NMR spectroscopy;[9, 10] however, since first introduced in the early 1990's,[11, 12] HDX-MS has become an increasingly attractive approach due to its ability to study large proteins and protein complexes at relatively low concentrations.[13-17] Solution-phase HDX-MS analysis of proteins is generally performed by measuring the mass-to-charge (*m*/*z*) shift of protein/peptide ions that occurs due to isotopic exchange between backbone amide hydrogens and the surrounding deuterium-rich solvent. In higher-order conformations, more structured and solvent inaccessible regions are protected from exchange compared to disordered and solvent accessible regions of the molecule[5]. The *m*/*z* shifts arising from isotopic exchange within the latter regions are currently exploited by HDX-MS to study structures of challenging systems[18-26] folding dynamics[27-31], protein-protein and protein-oligonucleotide interactions[32-40], as well as protein-ligand interactions and any associated conformational changes[41-49].

Over the years, various HDX-MS techniques/approaches have been developed to study the structures of proteins. One widely-applied method is that of "bottom-up" HDX-MS[50-54]. This approach takes advantage of the ability to localize exchange to specific protein regions using enzymatic digestion and subsequent determination of deuterium uptake within the generated peptides by MS measurements. A separate approach is to examine the deuterium labeling of the intact protein using MS. Indeed, "top-down" HDX-MS strategies have been described in which the labeled protein ions are subjected to tandem mass spectrometry (MS/MS) in order to determine the location of deuterium exchange[55-60]. Both bottom-up and top-down experiments can be accomplished using continuous- and pulsed-labeling strategies[61]. The former approach tracks protein structure evolution by monitoring the exchange behavior of all

conformer populations over extended times. The latter approach seeks to capture snapshots of protein conformations at given time points such as those associated with folding transitions[62, 63]. This is accomplished using a very short reaction time period (ms range). Combining techniques can result in powerful methods to study rapid events. For example, on-line quench-flow setups can monitor events occurring on the ms timescale[64, 65].

Although much effort has been extended in the application of HDX-MS for protein analysis, far fewer studies have been published related to higher-order structure in nucleic acids. Recently, Largy et al., described the suitability of native HDX-MS for structured oligonucleotides using G-quadruplex DNA as a model system which included the measurement of exchange behavior from the seconds to hours timescales with high reproducibility[66]. The experiments revealed that the HDX rates were independent of charge state and overall number of adducts; however, HDX rates were associated with the degree of hydrogen bonding. More recently, powerful data analysis/visualization tools have been developed for analyzing HDX-MS data collected for oligonucleotides[67].

Recently it has been proposed that HDX can be conducted in the droplets of the ionization source of the mass spectrometer[68, 69]. Remarkably, a theta capillary approach was demonstrated as a means to determine the rates of exchange associated with different amine hydrogens[70]. Subsequent studies employed the new technique of capillary vibrating sharp-edge spray ionization (cVSSI)[71, 72] to examine the in-droplet exchange behavior of small molecules with the goal of exploiting such to aid compound identification purposes[73, 74]. More recently, experiments were performed to determine whether or not in-droplet HDX could be used to obtain structural information for biopolymers[75]. A notable finding was that the exchange rates of backbone amide hydrogens in peptides could be increased by orders of magnitude compared with those from bulk solution. This is consistent with the observation that reactions confined to droplets can be dramatically accelerated as proposed in seminal studies[76-81]. Additionally, the

cVSSI experiments demonstrated that in-droplet HDX could be used to distinguish co-existing protein structures in solution[75].

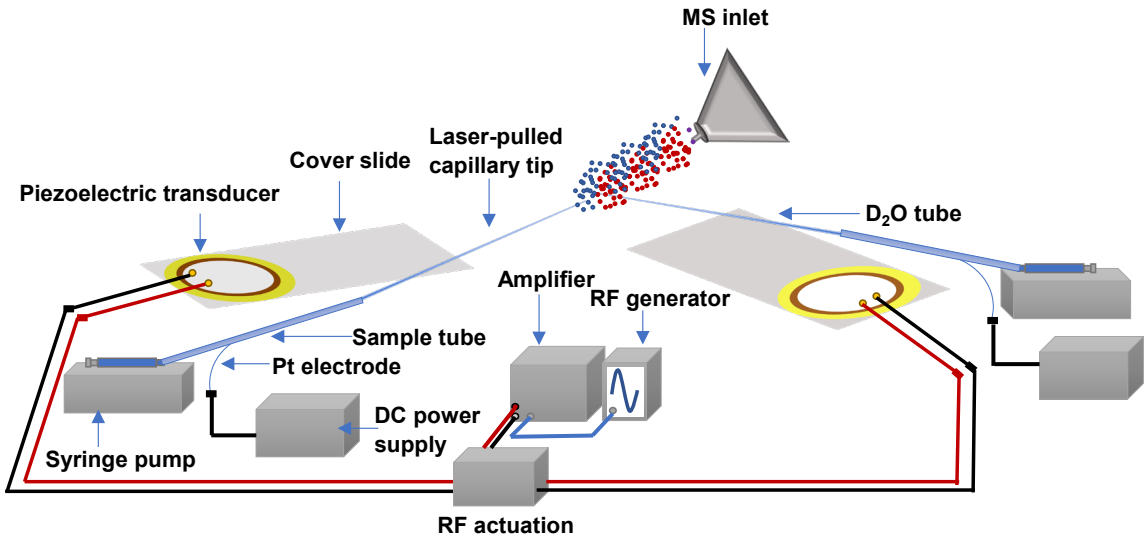

Figure 1. Schematic diagram of the dual cVSSI setup to study DNA structures. Required component parts to perform *in-droplet* HDX-MS experiments are labeled. The diagram is not drawn to scale.

In the present study, in-droplet HDX occurring on the microsecond time scale[70] is examined for its ability to distinguish various folding topologies of DNA molecules[82]. Here, not only is the rapid solution-phase HDX facilitated by cVSSI[73, 74], but also the ionization efficiency of the negatively charged ions[72]. To accomplish in-droplet HDX a dual spray emitter setup[73] is used as shown in Figure 1. In this approach, one emitter is used to charged droplets containing the analyte DNA while the other is used to create a plume of D_2O droplets. The ionization/reaction source setup as shown in Figure 1 is identical to that employed in protein analysis providing a reproducible and rapid droplet mixing/exchange strategy[75]. Here the approach is used to examine a number of single-strand, duplex, G-quadruplex, and triplex DNA species.

Overall, the in-droplet HDX experiments reveal that considerably different levels of deuterium uptake are observed for unfolded and folded forms of all structures including single-strand, duplex, G-quadruplex, and triplex DNA folding ensembles. The greatest variation in

exchange site protection is observed for the G-quadruplex cohort where a nearly 2-fold range in deuterium incorporation is observed. Notably, distinguishable exchange percentages are observed between Hybrid 1 and Hybrid 2 G-quadruplex conformations. Correlation analysis suggests that this rapid exchange process captures differences associated with base protection for the G-quadruplex ions.

Materials and methods

Chemicals and Reagents. All DNA oligonucleotides were purchased from Integrated DNA Technologies, Inc. (Coralville, IA, U.S.A.). High-performance liquid chromatography (HPLC) grade water, nuclease-free grade water, potassium chloride (KCl) and 1M triethylammonium acetate (TEAA) buffer solution, ammonium acetate, and deuterium oxide (D_2O) reagent were purchased from Fischer Scientific (NJ, U.S.A.). All chemicals and solvents were used without further purification.

Sample preparation. All single stranded DNA oligonucleotides were dissolved in nuclease-free water to prepare 100 μM stock solutions. For DNA duplexes, oligonucleotides were diluted to 10 μM with the appropriate amount of buffer to reach 100 mM ammonium acetate. Each diluted duplex-forming DNA sample was annealed by heating at 95 °C for 2-3 minutes then cooled to 4 °C and maintained overnight. For G-quadruplexes, 5 mM KCl stock solution was prepared in nuclease-free water and commercial 1M TEAA was used directly for the sample preparations. Each oligonucleotide was diluted to 10 μM with the appropriate amount of solution to achieve 1 mM KCl and 100 mM TEAA. Each diluted DNA sample was annealed by heating at 85 °C for 5-7 minutes then cooled to 4 °C and maintained overnight. The triplex DNA was prepared by adding $(GAA)_6$ and $(TTC)_6$ at a 1:2, respectively, molar ratio ultimately yielding 18mer GAA.TTC triplex DNA. For the HDX experiments the final concentration was 10 μM triplex DNA in 200 mM ammonium acetate. Triplex-forming DNA samples were annealed by heating the solution at 90 °C for 10 minutes followed by slowly cooling to room temperature. Next, the relevant amount of

internal standard (dT_6) was added to each sample solution to a final concentration of 1 μM. These solutions were then directly used for MS experiments without any further dilution.

For the experiments used to obtain HDX propensity values for each nucleotide, eighteen different stock solutions each containing a unique 6-residue oligonucleotide were created. The sequences were selected at random and are provided in Table S1 in the Supporting Information section. Each stock solution consisted of 100 μM oligonucleotide in nuclease free water. For HDX-MS experiments, each stock was diluted to 10 μM oligonucleotide in 100 mM ammonium acetate buffer. Additionally, an internal standard (dT_6) was added at a final concentration of ~3 μM.

Circular dichroism (CD) spectroscopy. In order to confirm the G-quadruplex topology, CD measurements were collected. CD spectroscopy is frequently used in many G-quadruplex studies[83, 84] because it provides information on the stacking configuration of the guanine bases (anti/syn). Because G-quadruplex topologies have specific stacking orientations, CD spectra secondarily provide information on strand orientation as well.

CD experiments were performed with a JASCO J-810 CD Spectrophotometer. The same DNA solutions used in the MS experiments were used here without any alteration in concentration. Each sample was scanned three times from 210-350 nm employing a scan speed of 50 nm·min.$^{-1}$ and 0.2 nm bandwidth. All spectra were collected at 20 °C. CD data were plotted as molar circular-dichroic absorption (Δε) vs. wavelength. Ellipticity values were normalized to Δε using Equation 1,

$$\Delta\varepsilon = 32980\,\theta \times c \times l \qquad 1),$$

where θ is the CD ellipticity in degrees, c is the DNA concentration in mol·L^{-1} (10 to 5 mol·L^{-1}), and l is the pathlength in cm (0.2 cm).

Fabricating cVSSI devices. The cVSSI devices were fabricated as described previously[71, 72]. Briefly, laser-pulled capillary emitter tips (fused silica, I.D. 100 μm, Polymicro Technologies, AZ, U.S.A.) were prepared using a P-2000 micropipette puller and chemically

etched using 30% hydrofluoric acid to achieve an end I.D. ranging between 10-15 μm. The capillary tip was attached to one end of a glass microscope cover slide (24 × 60 mm, VWR) and a piezoelectric transducer was attached to the other end of the same slide. The device was activated using a function generator (RIGOL DG-quadruplex102) and a power amplifier (Krohn-Hite 7500) employing a predetermined working frequency (92-96 kHz) and amplitude (80-140 mV_{pp}) as described previously[71, 72]. A PTFE tube (#30 thin-wall tubing, Cole-Parmer Instrument Company) was attached to the sample syringe and was also connected to the back of the emitter tip. To supply a bias voltage, a ~5-cm-long Pt wire was inserted into the PTFE tube allowing a conductor connection from a high-voltage DC power supply (HEOPS-10B2, Matsusada Precision Inc.).

For the larger oligonucleotide studies, analyte sample flow rates were maintained at 1 $\mu L \cdot min^{-1}$. A similar cVSSI device/tubing setup was used for the D_2O and the flow rate was maintained at 4 $\mu L \cdot min^{-1}$. For the study employing the 6-residue oligonucleotides, the analyte sample and D_2O reagent flow rates were each maintained at 10 $\mu L \cdot min^{-1}$.

Hydrogen-deuterium exchange. Two syringe pumps were used for the analyte solution and D_2O reagent in order to maintain independent flow rates. The DC voltage applied to the analyte solutions ranged from ~-1200 to ~-1400 V for each sample. A small voltage of ~-300 V was applied to the D_2O reagent to ensure consistent and efficient mixing[73]. The sample and D_2O emitter tips were placed 4 mm and 1 mm away from the MS inlet, respectively. These tips were arranged at a ~90° angle as shown in Figure 1 to facilitate the maximum HDX. This allowed analyte and reagent droplets to mix immediately prior to entering the mass spectrometer inlet.

Mass spectrometry. The MS measurements for quadruplex, duplex, and triplex forming oligonucleotides were carried out in negative-ion mode on a Q-Exactive hybrid Quadruple-Orbitrap mass spectrometer (Thermo Fisher, San Jose, CA). For the quadruplex and duplex oligonucleotides, full scan mass spectra ranging from 400 to 2000 *m*/*z* were collected using a resolving power setting of 70,000 and the capillary temperature was maintained at 275 °C. For

triplex oligonucleotides, the *m*/z range was set at 800 to 3000. The injection time was also increased from 500 to 2000 ms. This provided the best ion signal levels for these larger ions. All experiments were performed on the same day to ensure similar environmental conditions for the in-droplet HDX reactions. For initial data collection, the analyte tip was placed directly in front of the MS inlet (~4 mm away) without D_2O incorporation and total ion mass spectra were collected. Then, the D_2O tip was placed in the specified location (Figure 1) to allow HDX and again the resulting mass spectra were collected. Data were collected for 1 min. and obtained as triplicate measurements. Between replicate data collection, the RF and DC voltage supplies for the cVSSI devices were turned off and then on to assess/demonstrate performance reproducibility.

The MS measurements for the 6-residue oligonucleotides were collected on a linear ion trap mass spectrometer (LTQ XL, ThermoScientific). Here the *m*/*z* range was set at 800 to 1000. The injection time was maintained at 1000 ms with an AGC setting 1E6. The positioning of analyte and emitter tips was the same as that utilized for the larger oligonucleotides.

To account for plume fluctuations due to emitter tip positioning and factors such as small air currents, an internal standard (dT6) is utilized during the HDX experiments. Here, the *m*/*z* shift of the isotopic distribution of the internal standard is monitored as the emitter tip positions are slightly adjusted for all analytes. Upon achieving similar isotopic distributions for the internal standard after undergoing HDX, replicate datasets are recorded to determine the degree of solution deuterium incorporation in the analyte molecules.

Calculating the percent deuterium (%D) incorporation for oligonucleotide ions. The %D for each analyte molecule is determined using shifts in the weighted-average *m*/*z* value (m/z_{ave}) for the isotopic distributions of the oligonucleotide ions as described in detail previously[73]. To compare HDX reactivities among the different DNA structures, the %D values must be normalized according to the exchange level of the internal standard. For the internal standard, the %D is determined for the $dT6^{2-}$ ions in each mass spectral dataset. For all experiments reported here, the %D for the internal standard did not fluctuate significantly; values ranged from ~27% to ~32%

for the different solutions of the analytes. For HDX reactivity comparisons, the %D incorporation of each analyte was multiplied by the ratio $\frac{30}{x}$ where *x* represents the average %D incorporation for the internal standard ions.

The exchangeable sites of DNA oligonucleotides include hydrogens on the hydroxyl groups at the 5'- and 3'-termini, the backbone phosphate groups, and the heteroatom-bound hydrogens of the nucleobases. At physiological pH, backbone phosphate groups are deprotonated due to their acidity (low pK_a value); however, in negative ion mode ESI-MS experiments, many backbone phosphate groups in oligonucleotides are observed as neutral moieties while a smaller number are deprotonated and contribute to the observed charge of the analyte ions. Additionally, fully-folded G-quadruplex conformers contain K^+ ions comprising those required to stabilize the stacked tetrads. The number of K^+ ions is one less than the total number of tetrads (*N*). Therefore, for %D incorporation calculations, selected charge states must be considered to have *N*-1 extra sites of deprotonation to account for these cations. Thus, in the calculation of the %D incorporation for a three tetrad species having charge states 5^-, 6^- and 7^-, a total of 7, 8, and 9 hydrogens, respectively, are subtracted from the neutral molecule to represent the total available for exchange. In contrast, for the DNA duplex and triplex ions, the number of available hydrogens is simply the neutral compound value minus the charge state number.

Determining the nucleotide HDX propensity parameters. To determine the contribution to exchange by each nucleotide within an unstructured region of a larger oligonucleotide, a technique similar to that employed for amino acid residues was utilized[75]. Briefly, the %D incorporation for the twenty 6mer oligonucleotides served as the vector input for multiple regression analysis while the numbers of each nucleotide within individual 6mer sequences served as the 4×20 matrix input. Multiple regression was conducted using an online calculator[85] where the significance level was set at 0.05 and the y-intercept was set to zero. The output

provided coefficients for each nucleotide type (A, C, G, T) representing its average contribution to HDX for the multiple measurements.

Results and Discussion

Oligonucleotide selection. G-quadruplex structures in nucleic acids are non-canonical, four-stranded structures formed in guanine-rich sequences [86]. G-quadruplex can be formed from DNA, RNA, LNA and PNA molecules [87-89]. These sequences are found to be clustered in the human telomeric region where repetitive guanine-rich sequences are observed. Additionally, such regions are preserved which indicates the functional importance of these motifs in human evolution[90]. Moreover, human telomeric sequence is one of the first discovered and most extensively studied quadruplex-forming sequences in genomic DNA[91]. The building block of G-quadruplexes are G-quartets where four guanine bases form a cyclic conformation through Hoogsteen hydrogen bonds. These planar G-quartets stack on top of one another to form a four-stranded quadruplex structure[92-94]. Such structure is stabilized by intercalating monovalent metal cations such as Na^+, K^+ *etc*[95, 96]. Within the tetrad structure, guanine residues may adopt either a syn or an anti-glycosidic conformation. Because of this characteristic, G-quadruplex DNA structures are highly polymorphic and exhibit parallel, antiparallel, and hybrid topologies[97] as shown in Figure S1 in the Supporting Information section. Depending on the loop arrangement, the hybrid conformer is divided mainly into two subtopologies namely, hybrid-1 and hybrid-2 (Figure S1A and S1B, respectively)[84] The folding of these quadruplex topologies is dependent on the sequence, associated metal cation, flanking bases, position of the loop, salt concentration, and solution pH and ionic strength. The sequences of the G-quadruplex molecules studied here are provided in Table S2 in the Supporting Information section.

Triplex DNA is another type of non-canonical DNA which forms through binding of a triplex forming oligonucleotide (TFO) within the major groove of a duplex DNA namely triplex target sequence (TTS)[98]. The hydrogen bonding between the bases of TFO and TTS does not

constitute classical Watson-Crick base pairing, rather Hoogsteen hydrogen bonding involving purine-pyrimidine (N7-N3) interaction and either Thymine-Guanine (N6-O6) or Guanine-Cytidine (O4-N4). Thus, to form a triplex DNA structure, a repeating purine (Adenine and Guanine) stretch is required in the triplex target sequence to allow the formation of Hoogsteen hydrogen bonding. Several biological applications have been proposed for triplex DNA. The selection of the triplex DNA as well as the duplex DNA is intended to provide a stark structural comparison to the G-quadruplex species. Whereas the latter form structures that are similar in some respects to globular proteins having compact cores, the latter provide linear conformations. This allows the comparison of globular species with more linear molecules.

Verification of Quadruplex DNA structure. In order to examine the utility of in-droplet HDX to distinguish different DNA conformers, it is necessary to verify that the structures were formed during the annealing process. This is relatively straightforward for duplex and triplex species as the mass spectra reveal the favoring of duplex and triplex ions (absence of single strand DNA ions). For the single-strand quadruplex species, structure verification in this manner is not possible. Therefore, each quadruplex sample was examined using CD spectroscopy to ensure the correct topology. Figure 2 shows CD spectra representing each topology studied here. Briefly, for illustration, the CD spectrum of a parallel G-quadruplex structure (Figure 2A) showed a maximum at 260 nm. This results from the fact that this topology only has anti/anti-stacking orientations. In contrast, an anti-parallel G-quadruplex topology (Figure 2B) has both anti- and syn- guanines that are stacked alternatively. Thus, the CD spectra of the anti-parallel topology showed a minimum at 260 nm and maximum at 290 nm. The hybrid topology (Figure 2C) showed two maxima at 270 and 290 nm because both anti/syn and anti/anti stacking orientations exist for this topology. Between the two hybrid 1 topologies, 24TTG and 23TAG, the molar circular-dichroic absorption ($\Delta\varepsilon$) is lower for 23TAG (Figure S2 in the Supporting Information section). Decreased absorbance indicates a lower proportion of the quadruplex in solution and thus decreased solution folding for 23TAG. The difference between these two hybrid-1 topologies will

be discussed below. Notably, the relevant CD spectral patterns were observed for each of the quadruplex samples and are shown in Figure S2 in the Supporting Information section.

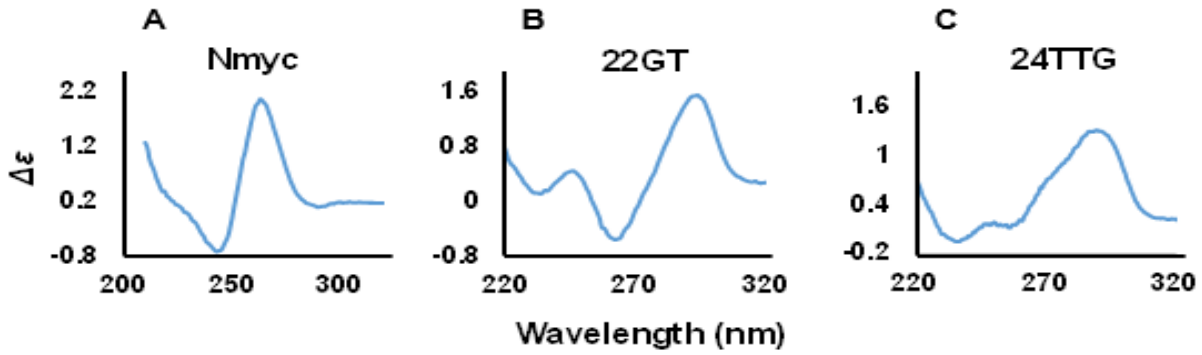

Figure 2. CD spectra of representative G-quadruplex topologies. Shown are spectra for Nmyc (parallel, A), 22GT (antiparallel, B) and hybrid-1 (24TTG, C). All DNA quadruplex solutions are maintained under the same conditions used for the MS experiments (i.e.,10 uM DNA concentration in 100 mM TEAA and 1 mM KCl).

Determining deuterium incorporation of G-quadruplex DNA. Figure 3 shows representative mass spectra for G-quadruplex ions before and after activation of the D_2O reagent cVSSI device. Briefly, for 5^- 24TTG ions, a shift in m/z_{ave} (1529.2 to 1530.7) is observed as shown in Figure 3C and 3D; this corresponds to an average deuterium uptake value of ~8.7. Similarly, for the same charge state for 23TAG the shift corresponds to an uptake value of ~15.7 (Figure 3E and 3F). Using the sum of all exchangeable hydrogens (neutral phosphate groups, imino and amino hydrogens, and hydroxyl groups at molecular termini) these deuterium uptake values represent %D incorporation levels of ~12.1% and ~22.6% for the respective sequences.

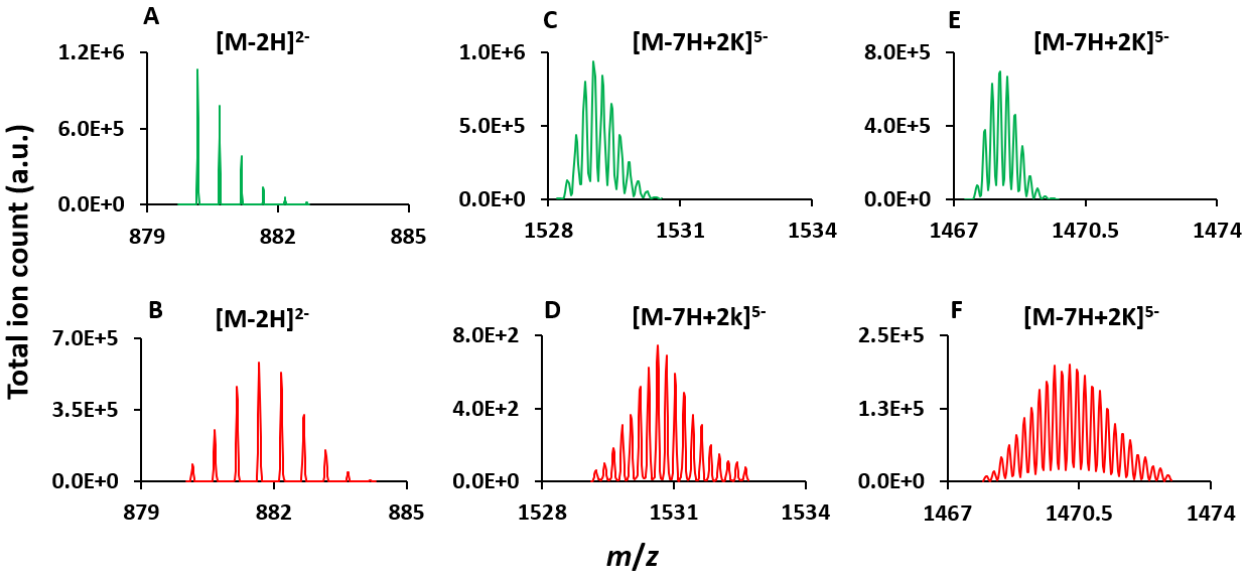

Figure 3. Mass spectra for representative analytes. The green colored isotopic distributions (A, C, and E) represent conditions before deuterium incorporation. The red colored distributions (B, D, and F) represent conditions for deuterium incorporation. Results are shown for the internal standard dT_6 (A, B), 24TTG (C, D) and 23TTG (E, F) ions. Here the zoomed regions represent the $[M\text{-}2H]^{2-}$ and $[M\text{-}7H+2K^+]^{5-}$ ions for the internal standard and G-quadruplex species, respectively. The G-quadruplex ions are those containing two K^+ adducts.

To compare the reactivities of the different conformers, the average %D incorporation was determined using multiple charge states. Additionally, the %D incorporation has been determined for unfolded forms of each analyte. The unfolded forms were obtained by not subjecting the DNA to the annealing process. Table 1 provides the %D incorporation values determined for all experiments reported here. Overall, the average %D uptake for unfolded single strand DNA is very similar exhibiting an average value of 23±2%. For the annealed G-quadruplex structures, in every case, the %D incorporation is less than that obtained for the unfolded molecules. Overall, the average %D incorporation for the folded structures is 18±3%. This represents an increase in hydrogen site protection of ~22% on average indicating that the folded structures provide some protection for specific exchange sites.

Table 1. Percent deuterium uptake of DNA species

Oligonucleotide ID	Average percent deuterium uptake	
	Unfolded conformer	Folded conformer
DK66	24.6 ± 0.4[a]	17.8 ± 0.5[b]
DK66*	24.8 ± 0.3[a]	18.3 ± 0.1[b]
24TTG	23 ± 1[c]	12.4 ± 0.2[d]
23TAG	22.1 ± 1.2[c]	19.5 ± 0.5[d]
26TTA	23 ± 1[c]	18.1 ± 1.5[c]
Bcl-2	23.1 ± 1.9[c]	18.4 ± 1.5[c]
VEGF	22.2 ± 0.6[c]	17.7 ± 1.1[c]
Nmyc	21 ± 1[c]	15.5 ± 1.6[c]
T95 2T	24.8 ± 1.3[c]	16.6 ± 1.4[e]
22CTA	23.9 ± 0.6[c]	20.5 ± 0.6[c]
TBA	25 ± 2[c]	21.0 ± 0.4[c]
21GT	24.1 ± 0.8[c]	20.8 ± 1[c]
5-TET	18.4 ± 0.6[c]	15.5 ± 1.0[c]
18 GAA, 18 TTC; 18 mer triplex	26.7 ± 0.3[f], 22.2 ± 0.7[f]	16.1 ± 0.9[g]

[a]Average uptake of charge states 3^- and 4^-.
[b]Average uptake of charge states 4- and 5-.
[c]Average uptake of charge states 4-, 5-, and 6-
[d]Average uptake of charge states 5-, 6-, and 7-.
[e]Average uptake of charge states 3, 4 and 5.
[f]Average uptake of charge state 4.
[g]Average uptake of charge states 6 and 7.

Comparison of exchange site protection by G-quadruplex conformers. Having demonstrated that the G-quadruplex structure formation provides some protection of exchange sites, a question arises as to whether or not the separate conformers afford significantly different levels of exchange site protection. Figure 4A shows the relationship between the deuterium

uptake levels for the folded and unfolded forms of the G-qaudruplex molecules. The overall correlation is relatively low exhibiting a R^2 value of 0.32 suggesting variability in the protection afforded by different G-quadruplex topologies. A noticeable difference is clearly observed in Table 1 within the hybrid structural types. Here 24TTG exhibits a %D incorporation that is ~34% below the average of the other three quadruplex species (23TAG, 26TTA, Bcl-2). This difference will be discussed in greater detail below.

Excluding the results for 24TTG, a cursory examination of Table 1 suggests that the hybrid, parallel, and antiparallel topologies do provide significantly different levels of protection where the order of protection is parallel>hybrid>antiparallel. To verify this, a series of T-tests have been performed using the %D incorporation data for the different topologies. For the hybrid/parallel, parallel/antiparallel, and hybrid/antiparallel comparisons, p-values of 1.9×10^{-4}, 9.4×10^{-10}, and 3.2×10^{-5} have been obtained. Thus, it may be suggested that in-droplet HDX can, to some degree, distinguish different topologies.

Hydrogen type protection of G-quadruplex structures. Having noted the differences in HDX reactivities for the different topologies, it is instructive to ask how the formation of globular-like structure effects protection of different exchange sites for the hybrid, parallel, and antiparallel topologies. One method to attempt to deduce the types of hydrogens that become protected is to perform correlation analyses. Using the various sequences of the DNA G-quadruplex structures, the deuterium incorporation can be compared with the numbers of available hydrogens based on hydrogen site type.

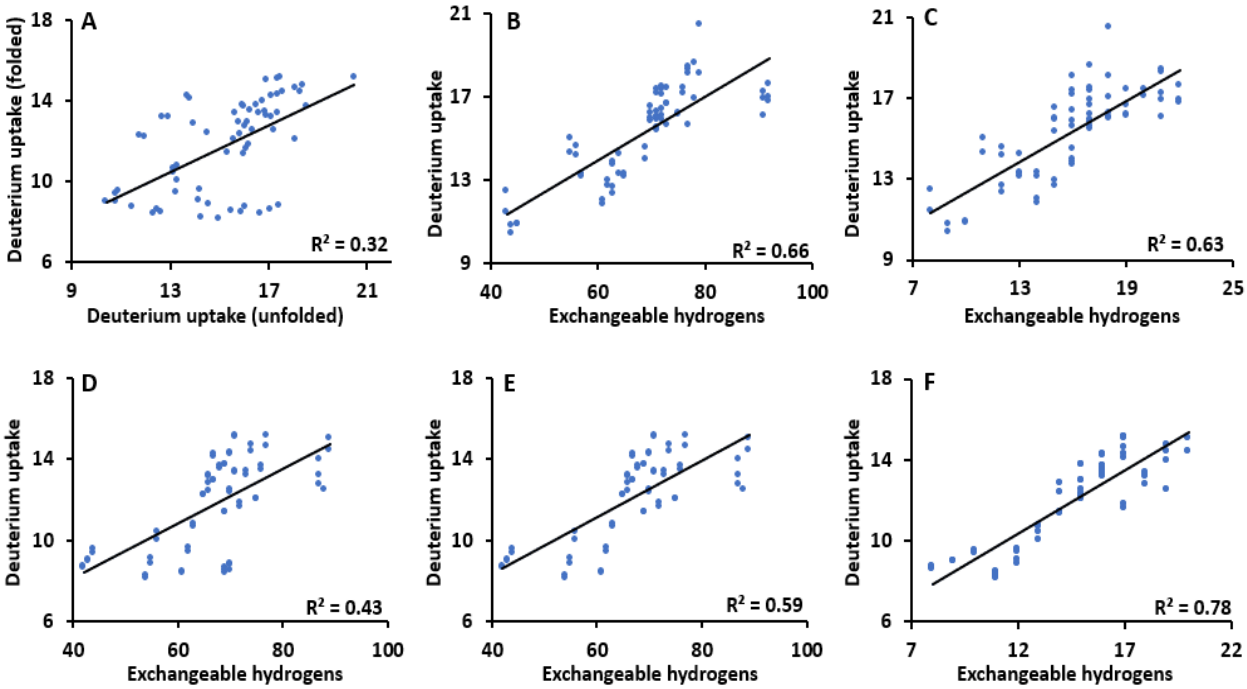

Figure 4. Correlation plots showing deuterium uptake dependence. Panel A shows the correlation for total experimental deuterium uptake for unfolded structures versus their corresponding folded G-quadruplex species. For panels B, C, D, E, and F, the *x*-axis represents the number of exchangeable hydrogens and the *y*-axis represents the experimental deuterium uptake. For unfolded molecules, panels B and C show the relationship of deuterium uptake with all of the exchangeable hydrogens and those on neutral phosphates only, respectively. Panel D, E, and F show the results obtained for the folded G-quadruplex species. For panels D and E, the exchangeable hydrogens are all heteroatom hydrogens and all such hydrogens while rejecting the outlier (24TTG). Panel E shows the relationship when the exchangeable hydrogens are limited to neutral phosphate sites.

The first comparison of deuterium incorporation with hydrogen type is shown in Figure 4. Here, for unstructured molecules, the deuterium incorporation is shown to increase with the total number of exchangeable sites (Figure 4B). A R^2 value of 0.66 is obtained for the best-fit line. When the x-axis is reduced by including only exchangeable hydrogens from neutral phosphate sites (Figure 4C), the strength of the correlation with total deuterium uptake is not changed appreciably. That is, the R^2 value remains largely unchanged at 0.63. From the comparison of the two correlation plots (Figures 4B and 4C) it can be argued that there is no indication that there is no evidence for favored exchange of backbone or base hydrogens.

In separate analyses, the dependence of deuterium incorporation on the numbers of available hydrogens has been assessed for the folded G-quadruplex species. The results are shown in Figures 4D, 4E and 4F. For these molecules, the best-fit line for total deuterium uptake

versus total number of exchangeable sites (Figure 4D) provides a R^2 value of 0.43. This correlation is weaker than that obtained for the unfolded molecules (Figure 4B) suggesting possible protection that is related to hydrogen type. Note that for a comparison that excludes results for 24 TTG (Figure 4E) due to its unusual level of hydrogen protection (discussed below), a better correlation is obtained (R^2 = 0.59); this value is still below that obtained for the unfolded forms (Figure 4B). However, a significant difference in correlation strength is encountered for the analysis comparing deuterium uptake with neutral backbone sites (Figure 4F). Here, the correlation is improved and a R^2 value of 0.78 is obtained. The latter value is the strongest correlation obtained for all G-quadruplex comparisons. This would suggest that upon folding, solvent accessibility is lost to some of the base hydrogens but not the backbone sites. This is consistent not only with tetrad formation, but also the preservation of such structure even at the late stages of the ionization process. This is also consistent with the previous argument that the quadruplex structure is preserved into the gas phase environment during the ionization process[99].

Multiple regression analysis supporting guanosine base protection. Separate HDX-MS analyses of twenty random 6mer DNA sequences has provided deuterium uptake levels that can be used to obtain HDX propensity values (or HDX parameters) in a manner described previously for other small molecules[74, 75]. A representation of typical data collected for the 6mer DNA sequences (Table S1 in the Supporting Information section) is shown in Figure S3 in the Supporting Information section. From these analyses, the parameters for nucleotides C, A, T, and G are 1.16 (p = 6.1E-5), 1.36 (p = 9.2E-6), 0.35 (p = 0.30), and 0.63 (p = 0.02), respectively. As a first approximation, for in-droplet reactions, these values would represent the relative differences in HDX contribution by individual nucleotides in unstructured regions of larger oligonucleotides. As an indication of the utility of the calculation, consider that the correlation between predicted deuterium uptake and experimental uptake is significantly improved for the eighteen sequences using the parameters as described previously[74]. Here, the R^2 value

associated with the predictions improves from 0.24 to 0.65 as shown in Figure S4 in the Supporting Information section when the parameters are used compared with treating all hydrogens equally.

The HDX parameters can be utilized on the unfolded and folded forms of the G-quadruplex species. The R^2 value for the predicted exchange versus experimental exchange for the unfolded G-quadruplex species is determined to be 0.61 as shown in Figure S5A in the Supporting Information section. This is very close to that obtained for the correlation applied to the 6mer oligonucleotides (Figure S4B in the Supporting Information section). That the parameters do as well, comparatively, for predictions for the much larger unfolded G-quadruplex species suggests that they do to some extent reflect nucleotide HDX reactivity differences associated with unstructured regions. When the same parameters are applied to the folded G-quadruplex species, the R^2 value associated with the best-fit line for predicted versus experimental uptake decreases to 0.35 as shown in Figure S5B in the Supporting Information section.

That the folded G-quadruplex species are not well predicted by the contributions of the free oligonucleotides suggests that the G-quadruplex protection observed in the experimental data may be associated with specific residues. Figure S6A in the Supporting Information section shows that when the hydrogens of the guanosine nucleotides associated with tetrads are removed from the correlation calculation, the R^2 value changes from 0.35 to 0.46. This is better than that achieved from a random removal of hydrogens for the same number of nucleotides where the R^2 value only improves to 0.38 (Figure S6B). Although not conclusive, this analysis is here presented as supporting the idea that the different protection levels observed for G-quadruplex species subjected to in-droplet HDX arises in part due to the protection by the hydrogen bonding of the tetrads. As mentioned above, such an observation cannot account for all differences such as that observed for 23TAG and 24TTG.

G-quadruplex toplogy-specific protection. As observed in Table 1, The hybrid-1 G-quadruplex species 24TTG provides the greatest degree of protection for all folded structures.

The hybrid-2 species (26 TTA and Bcl-2) both exhibit higher levels of %D incorporation. It may be possible that these hybrid-2 species exhibit greater overall flexibility than 24TTG and thus exchange site accessibility for these rapid HDX experiments. Caution should be noted with such an interpretation as recent native MS studies have suggested that droplet conditions may result in enhanced dynamics for some biopolymers and the dataset presented here is too small to make definitive distinctions regarding flexibility[100]. Also, such an argument does not account for the %D incorporation difference for hybrid-I 24 TTG and 23 TAG structures. 23TAG is a natural human telomeric DNA sequence, available as ~60% to 70% hybrid-1 in K^+ solution[101]. Therefore, the greater structural polymorphism in the solution could result in greater solvent exposure to exchange sites ultimately leading to the highest %D incorporation. Comparatively, 24TTG is a modified telomere sequence. It is formed by modifying the two residues at the 5' terminal of 23TAG which drives the structural equilibrium to 95% hybrid-1 in K^+ solution. These experiments show that the "monomorphic" 24TTG quadruplex exhibits very low levels of %D uptake. Similarly, 26TTA differs from 23TAG only by 3 terminal residues, which favors >80% hybrid 2 conformer formation[102]. This conformer also yielded a distinctively higher %D incorporation. Bcl-2, which is not a derivative of 23TAG, but available as ~90% Hybrid-2 in solution showed very similar HDX behavior to that of 26TTA. These preliminary results suggest that structural flexibility and transformations in solution may yield %D incorporation differences as captured by in-droplet HDX.

In comparison to the hybrid topology (23TAG, 26TTA, and Bcl-2), the parallel topology (VEGF, Nmyc, and T95 2T) shows increased protection. Separate studies of these structures in different solvent systems have shown that, on average, these parallel structures exhibit higher melting point temperatures (T_m) values than the hybrid structures. So, with the caveat that droplet and charge contribution to flexibility remain largely unknown, it may be suggested that the decreased levels of deuterium incorporation for parallel structures arise to some degree as a result of the increased stability (decreased flexibility) of the solution conformers. In comparison,

the antiparallel topologies contain only two tetrads whereas the other species contain 3 to 5. It is likely that the larger globular core formed by the 3 to 5 tetrad species imparts greater protection to exchange. Additionally, for the 22CTA and 21GT species, a lower proportion of bases (percentage of the total sequence) is involved in tetrad formation compared with the hybrid and parallel topologies. This observation further strengthens the argument that in-droplet HDX distinguishes conformers based on tetrad protection. Comparatively, the behavior of the TBA G-quadruplex molecule could not be described in this manner as it is only 15 residues in length.

Comparison of duplex and quadruplex DNA. Having described the HDX behavior of DNA species that form relatively globular structures, it is instructive to consider the exchange behavior of linear molecules. To investigate the relative protection offered by DNA duplex formation, data were recorded for 2 isomers (DK66 and DK66*). These molecules are 12-mer, self-complementary DNA oligonucleotides. DK66, which is also known as Dickerson's dodecamer is a prototypic B-DNA that has been extensively studied[103]. Upon performing cVSSI of the single-strand species, similar charge state distributions were observed. Additionally, similar levels of %D incorporation were observed for these unfolded molecules; deuterium uptake values of 24.6 ± 0.4% and 24.8 ± 0.3% were calculated for DK66 and DK66*, respectively. After performing the annealing step to generate DNA duplex, the %D incorporation recorded for the respective duplex ions was 17.8 ± 0.5% and 18.3 ± 0.1%. Therefore, formation of the DNA duplex structure imparts protection to some of the rapidly exchanging sites accessed by in-droplet HDX; the %D incorporation decreased by ~28% and ~26% for DK66 and DK66*, respectively.

A comparison of the %D incorporation for DNA duplex and G-quadruplex structures suggests some differences in the degree of protection. A cursory examination of Table 1 suggests that the G-quadruplex species that most closely match the protection level presented by DNA duplex are the hybrid structures with the exception of the outlier 24TTG species (see discussion above). A t-test analysis shows that the protection levels for the DNA duplex and hybrid G-quadruplex structure are not significantly different at the 95% confidence limits ($p = 0.7$). In

contrast, t-tests show that the parallel and antiparallel structures exhibit protection levels that are significantly different at the 95% confidence limits (p = 2.6E-3 and 2.8E-11, respectively).

Based on the results of the correlation and multiple regression analyses for the G-quadruplex species, it can be argued that the origin of the exchange site protection for the DNA duplex arises from the hydrogen bonding of the base pairs. That said, it is noted, the fraction of residues involved in hydrogen bonding for the G-quadruplex tetrads is 0.5 ± 0.1 on average. In comparison, for DNA duplex, every residue is considered to be involved in hydrogen bonding. Therefore, it may be possible that some protection of the globular G-quadruplex species occurs at backbone sites especially for the parallel and hybrid structures which exhibit increased and similar levels of protection, respectively. That said, it is recognized that this is a very limited dataset, and any such conclusions would have to be verified from more extensive studies. Here, it is presented as one possibility for the exchange protection afforded by the globular-type structures.

Comparison of triplex DNA and quadruplex DNA. Having analyzed in-droplet HDX of DNA quadruplex and duplex molecules, the HDX behavior for the much larger non-canonical DNA triplex was examined for comparison purposes. Here, a DNA triplex molecule that is 2 to 4.5× larger than that of all DNA quadruplex and duplex species is considered; the mass spectra showing preservation of triplex DNA structure is presented in Figure S7 in the Supporting Information section. The triplex DNA consists of a 18-residue GAA triple repeat as well as its complementary 18-residue TTC sequence which bind through Watson-Crick hydrogen bonding; a third triplex forming TTC sequence completes the DNA triplex molecule through Hoogsteen hydrogen bonding after an annealing process. The HDX behavior for DNA triplex and constituent strands is shown in Figure 5. The DNA triplex exhibits 16.1 ± 0.9% D uptake which is significantly lower than its constituent single stranded sequences (GAA- and TTC-containing); the respective unfolded sequences have %D uptake values of 26.7 ± 0.3% and 22.2 ± 0.7%. From Table 1, it is evident that the DNA triplex molecule showed significantly greater protection than the antiparallel

DNA quadruplex species. A statistical t-test was performed to determine whether or not the DNA triplex protection level is significantly different from that of hybrid DNA quadruplex species. From the analysis, a p-value of 1.9E-4 suggests that DNA triplex provides significantly greater protection than the hybrid DNA quadruplex molecules. As before, the outlier 24TTG was excluded from this calculation. In contrast, the parallel DNA quadruplex and 5-TET molecules show similar levels of protection as that obtained for the DNA triplex.

Comparison of DNA triplex and DNA duplex molecules. A major structural difference between the DNA duplex and triplex molecules is that the latter contains an additional TFO sequence which binds to the major groove of the DNA duplex by Hoogsteen hydrogen bonding. Table 1 shows that the DNA duplex produces a higher %D uptake. The increased protection of afforded by DNA triplex is ~11% greater than that of the duplex DNA. As every residue on the TFO sequence also participates in Hoogsteen hydrogen bonding, it may again be suggested that a degree of backbone protection occurs. That said, it may also be the case that the addition of the TFO may prevent a greater amount of D_2O from accessing the structural core (hydrogen bonded bases). This presents the intriguing idea that rapid in-droplet HDX can probe a change in structural flexibility associated with the DNA triplex molecules.

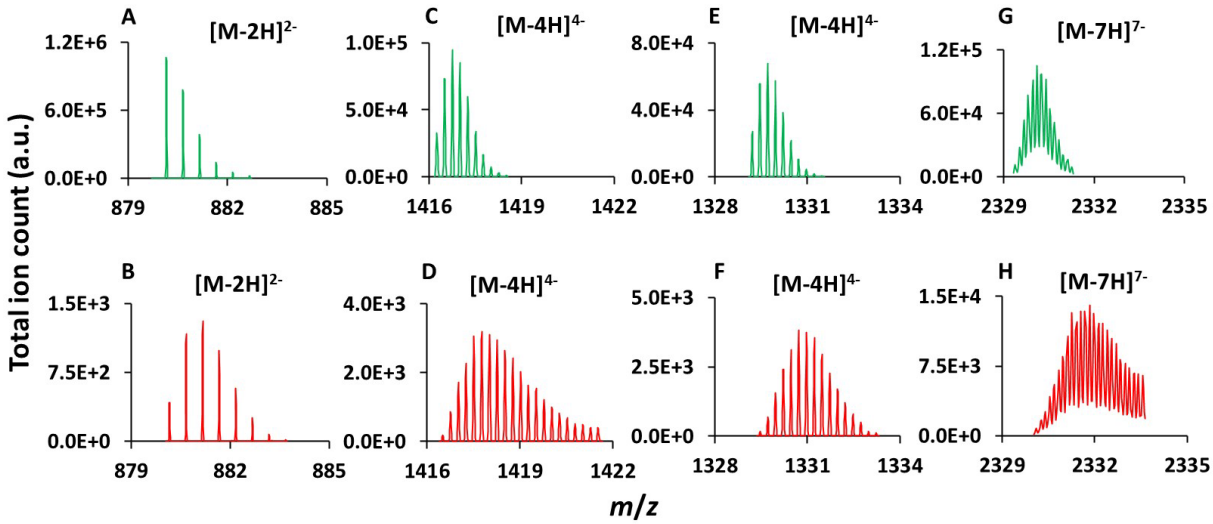

Figure 5. Isotopic distributions of 18-mer DNA species and the internal standard. Green colored mass spectra (Panels A, C, E, and G) show results prior to deuterium incorporation. The red colored spectra (Panels B, D, F, and H) represent data obtained upon deuterium incorporation. Results are shown for dT_6 (Panels A and B), 18GAA (Panels C and D), 18TTC (Panels E and F), and 18GAA.TTC triplex DNA (Panel G and H) ions. Here the zoomed regions represent the $[M-2H]^{2-}$ ions for the internal standard, $[M-4H]^{4-}$ ions for the ss 18GAA and ss 18TTC strands and the $[M-7H]^{7-}$ ions for the 18 GAA.TTC triplex DNA ions. Panels A, C, E, G show results obtained before the introduction of D_2O reagent and panels B, D, F and H show those after the introduction of D_2O.

Comparison to prior HDX results. It is instructive to compare the findings of these experiments with those obtained in prior HDX-MS investigations of G-quadruplex species. The previous work employing on-line HDX demonstrated that the backbone hydrogens were more accessible to exchange for the G-quadruplex DNA. Although less definitive, this also appears to be the case for all G-quadruplex species subjected to in-droplet HDX. The second finding of the prior study is that the HDX rate (and ultimately the number of unexchanged sites, NUS) is highly dependent on the degree of tetrad formation; the NUS after ~300 seconds exposure increased in order from two tetrad to five tetrad species. Although with in-droplet experiments it is not currently possible to obtain HDX kinetics information, the degree of deuterium incorporation on the microsecond timescale also showed a similar ability to distinguish molecules based on the number of tetrads in G-quadruplex species where those containing smaller numbers of tetrads show greater reactivity. Additionally, the prior studies suggested that for species containing three tetrads, the parallel topologies generally exhibited higher NUS after ~300 seconds exposure than the hybrid structures. This is consistent with the findings reported here for three of the hybrid

species and the parallel species. Finally, for 24TTG, the NUS after ~300 seconds exposure is significantly higher than 23TAG and 26TTA hybrid species. This is consistent with the significantly greater protection afforded by the 24TTG species observed here on the microsecond timescale. The only notable difference is the behavior observed for the Bcl-2 hybrid G-quadruplex topology; in the prior studies, the NUS after ~300 seconds exposure is closer to the that of 24TTG than the other hybrids studied here. Here, the exchange level is similar to 23TAG and 26TTA. In summary, for the most part, the findings on the microsecond timescale are very similar to those observed for long timescale measurements.

Future directions. The current experimental apparatus/setup to conduct microsecond HDX-MS is arguably very robust; Table S3 in the Supporting Information shows HDX results for DNA oligonucleotides obtained on a separate day using different cVSSI devices. Overall, %D values are within 0.6 ± 0.5 of those reported in Table 1. That said, the use of in-droplet HDX to distinguish different oligonucleotide structures as well as to elucidate structural information about specific topologies requires further development work.

The first area to consider is whether or not the methodology can be used to reveal the presence of coexisting structures as has been demonstrated for proteins. Such a capability would find utility in DNA folding studies using a quench flow type approach. Here, the in-droplet HDX could be used for rapid pulse labeling to reveal different coexisting structures along an initiated folding pathway. To accomplish this, a methodology to increase the amount of D_2O reagent may be required. From the unfolded conformer data (Table 1) it can be argued that the highest efficiency to be achieved may be ~25%. Although our previous studies demonstrated that the bulk of the HDX occurs in solution, a small amount of gas-phase exchange cannot be ruled out. For low levels of overall solution exchange, gas-phase exchange may be more problematic for distinguishing structures and obtaining structural information. Two different procedures can be investigated to increase the D_2O reagent available to the analyte molecules. First, the flow rate can be increased to the current D_2O reagent cVSSI device. This will lead to the production of a

larger number of droplets of the same size. Additionally, cVSSI devices of larger diameter can be employed to increase the overall size of the D_2O droplets. A goal would be to increase the ion liberation droplets to >50% D_2O.

With the advance toward distinguishing coexisting structures is the need for better mass informatics tools. A recent article describes the OligoR tool reported by Largy and Ranz[104]. The tool is able to deconvolute isotopic distributions from different conformer populations in a robust manner. In the prior study employing in-droplet HDX for proteins, a simple Gaussian fitting approach was employed as a first approximation of different conformer exchange levels. Should the improved in-droplet HDX experiments reveal coexisting structures, tools such as this will be invaluable for obtaining structure information. Another argument for improved data deconvolution can be observed from the data shown in Figure 5H. Here, the isotopic distribution used to calculate the m/z_{ave} does not achieve baseline at the higher end. This results from a merging of the deprotonated ions with those containing a single Na^+ adduct. Although, the use of the lowest midpoint between peaks serves as a good first approximation of exchange level, better tools will help to elucidate structural information in the future.

A second area that should be investigated is the use of ion fragmentation techniques to determine the locations of deuterium incorporation. Although collision-induced dissociation (CID) does not lend itself well to determining the sites of deuterium incorporation due to H/D scrambling, there are several ion fragmentation techniques which may find utility in determining the locations of accessible sites in negative ion mode. These include those that involve the formation of radical ion species. Two examples include charge-transfer dissociation (CTD) and negative electron transfer dissociation. The potential complementarity of these ion fragmentation techniques and the cVSSI approach cannot be overstated. cVSSI is shown to provide robust ion signal levels (>10 fold improvements relative to ESI)[72] that when coupled with negative ion fragmentation could provide first-of-its-kind structural information for oligonucleotide species. As one example, consider that although the HDX data here did not reveal the presence of multiple conformations,

MS/MS interrogation of different isotopologues may reveal the presence of such species with similar overall reactivities. This would be determined by localizing the deuterium uptake to different regions on the molecules.

Finally, the in-droplet HDX approach is straightforward to implement on any mass spectrometer that employs elesctrospray ionization (ESI)[105] ranging from gas-assisted nebulization to nanoelectrospray ionization (nESI)[106, 107]. As such, the method can be coupled to instruments that utilize physical probes of ion structure such as ion mobility spectrometry (IMS). One intriguing approach for investing the structures of biopolymers using IMS-MS measurements involves the controlled heating of gas-phase conformers to track structural transitions in the gas-phase[108, 109]. Recently, collision-induced unfolding (CIU) has been extended to the study of RNA oligonucleotides[110] revealing the preservation of elements of solution structure into the gas phase. Combining in-droplet HDX with a post-ionization characterization of structure and structural transformations would offer complementary information (reactivity and collision cross sections) that can more fully characterize oligonucleotide structure. One clear advantage in using the cVSSI approach is the ≥10 fold enhancement in ionization efficiency compared with ESI and nESI for native MS experiments[72].

Conclusions

In-droplet HDX using a dual cVSSI setup combined with mass spectrometry was used to examine DNA structure in solution. The cVSSI setup was shown to provide robust ion signals for single-stranded unfolded and quadruplex species as well as duplex and triplex DNA. Overall, unfolded forms of the DNA sequences yielded the greatest %D incorporation values. Folded forms of the DNA molecules exhibited varying degrees of %D incorporation representing different levels of exchange site protection. For G-quadruplex DNA, HDX reactivity is shown to decrease with increasing numbers of tetrads. Additionally, for the species exhibiting three tetrads here, hybrid structures (with the exception of 24TTG) generally exhibited a decreased degree of

protection. For linear molecules, DNA duplex provided %D incorporation values that were similar to those of the three hybrid structures while triplex DNA showed increased levels of protection similar to the parallel and 5TET structures. Notably, for the hybrid 1 molecules, 24TTG provided the lowest level of deuterium incorporation (~12.4%) while 23TAG provided nearly the largest degree (~20%). This may be explained by the decreased propensity of the latter to form the hybrid 1 structure as well as increased conformational flexibility.

The ability to distinguish DNA folds using in-droplet HDX on the microsecond timescale is encouraging and should warrant fuller consideration of the use of the cVSSI technology for the study of oligonucleotide structure. For example, in the future, in-droplet HDX that takes advantage of the high-efficiency ionization by cVSSI may be used as a pulsed labeling approach to study other oligonucleotide folding such as i-motifs, RNA quadruplexes, DNAzymes and Ribozymes. In the post COVID world, such capability may prove valuable for improving human health.

Acknowledgments

The authors wish to acknowledge the financial support of this work by the National Science Foundation (CHE-1553021) and the National Institutes of Health (R01GM135432). We thank Dr. Callee Walsh (former manager of the WVU BNRF) for technical support and for access to the mass spectrometer and CD spectrophotometer instruments.

Conflicts Disclosure

The authors declare the following competing financial S.J.V. and P.L. have co-founded a start-up company, Invibragen Inc., to commercialize technologies involving vibrating sharp-edge spray ionization (VSSI).

References

[1] F. Wang, X. Tang, Conformational heterogeneity of stability of apomyoglobin studied by hydrogen/deuterium exchange and electrospray ionization mass spectrometry, Biochemistry, 35 (1996) 4069-4078.

[2] J.P. Hodkinson, T.R. Jahn, S.E. Radford, A.E. Ashcroft, HDX-ESI-MS reveals enhanced conformational dynamics of the amyloidogenic protein β2-microglobulin upon release from the MHC-1, Journal of the American Society for Mass Spectrometry, 20 (2009) 278-286.

[3] T.E. Wales, J.R. Engen, Hydrogen exchange mass spectrometry for the analysis of protein dynamics, Mass Spectrometry Reviews, 25 (2006) 158-170.

[4] S.W. Englander, Hydrogen exchange and mass spectrometry: A historical perspective, J Am Soc Mass Spectrom, 17 (2006) 1481-1489.

[5] M.M. Krishna, L. Hoang, Y. Lin, S.W. Englander, Hydrogen exchange methods to study protein folding, Methods, 34 (2004) 51-64.

[6] D.L. Smith, Y. Deng, Z. Zhang, Probing the non-covalent structure of proteins by amide hydrogen exchange and mass spectrometry, J Mass Spectrom, 32 (1997) 135-146.

[7] X. Hui, J.K. Hoerner, S.J. Eyles, A. Dobo, E. Voigtman, A.I. Mel'Cuk, I.A. Kaltashov, Mapping protein energy landscapes with amide hydrogen exchange and mass spectrometry: I. A generalized model for a two-state protein and comparison with experiment, Protein Science, 14 (2005) 543-557.

[8] I.A. Kaltashov, S.J. Eyles, Mass Spectrometry in Biophysics: Conformation and Dynamics of Biomolecules, 2005.

[9] S.W. Englander, Measurement of structural and free energy changes in hemoglobin by hydrogen exchange methods, Ann N Y Acad Sci, 244 (1975) 10-27.

[10] S.W. Englander, N.R. Kallenbach, HYDROGEN-EXCHANGE AND STRUCTURAL DYNAMICS OF PROTEINS AND NUCLEIC-ACIDS, Quarterly Reviews of Biophysics, 16 (1983) 521-655.

[11] V. Katta, B.T. Chait, Conformational changes in proteins probed by hydrogen-exchange electrospray-ionization mass spectrometry, Rapid Commun Mass Spectrom, 5 (1991) 214-217.

[12] Z. Zhang, D.L. Smith, Determination of amide hydrogen exchange by mass spectrometry: a new tool for protein structure elucidation, Protein Sci, 2 (1993) 522-531.

[13] T. Hofmann, S.A. Samsonov, A. Pichert, K. Lemmnitzer, J. Schiller, D. Huster, M.T. Pisabarro, M. von Bergen, S. Kalkhof, Structural analysis of the interleukin-8/glycosaminoglycan interactions by amide hydrogen/deuterium exchange mass spectrometry, Methods, 89 (2015) 45-53.

[14] J. Pan, S. Zhang, A. Chou, C.H. Borchers, Higher-order structural interrogation of antibodies using middle-down hydrogen/deuterium exchange mass spectrometry, Chem Sci, 7 (2016) 1480-1486.

[15] M. Benhaim, K.K. Lee, M. Guttman, Tracking Higher Order Protein Structure by Hydrogen-Deuterium Exchange Mass Spectrometry, Protein Pept Lett, 26 (2019) 16-26.

[16] B.A. Kochert, R.E. Iacob, T.E. Wales, A. Makriyannis, J.R. Engen, Hydrogen-Deuterium Exchange Mass Spectrometry to Study Protein Complexes, Methods Mol Biol, 1764 (2018) 153-171.

[17] R.A. Harrison, J.R. Engen, Conformational insight into multi-protein signaling assemblies by hydrogen–deuterium exchange mass spectrometry, Current Opinion in Structural Biology, 41 (2016) 187-193.

[18] G. Comamala, C.C. Krogh, V.S. Nielsen, J.P. Kutter, J. Voglmeir, K.D. Rand, Hydrogen/Deuterium Exchange Mass Spectrometry with Integrated Electrochemical Reduction and Microchip-Enabled Deglycosylation for Epitope Mapping of Heavily Glycosylated and Disulfide-Bonded Proteins, Analytical Chemistry, 93 (2021) 16330-16340.

[19] A.F. Clouser, Y.H. Alam, W.M. Atkins, Cholesterol Asymmetrically Modulates the Conformational Ensemble of the Nucleotide-Binding Domains of P-Glycoprotein in Lipid Nanodiscs, Biochemistry, 60 (2021) 85-94.

[20] K.W. Anderson, C. Bergonzo, K. Scott, I.L. Karageorgos, E.S. Gallagher, V.S. Tayi, M. Butler, J.W. Hudgens, HDX-MS and MD Simulations Provide Evidence for Stabilization of the IgG1-Fc gamma RIa (CD64a) Immune Complex Through Intermolecular Glycoprotein Bonds, Journal of Molecular Biology, 434 (2022).
[21] T.R. O'Leary, D. Balasubramaniam, K. Hughes, D. Foster, J. Boyles, K. Coleman, P.R. Griffin, Hydrogen-Deuterium Exchange Epitope Mapping of Glycosylated Epitopes Enabled by Online Immobilized Glycosidase, Analytical Chemistry, (2023).
[22] M.K. Cieplak-Rotowska, K. Tarnowski, M. Rubin, M.R. Fabian, N. Sonenberg, M. Dadlez, A. Niedzwiecka, Structural Dynamics of the GW182 Silencing Domain Including its RNA Recognition motif (RRM) Revealed by Hydrogen-Deuterium Exchange Mass Spectrometry, Journal of the American Society for Mass Spectrometry, 29 (2018) 158-173.
[23] R.C. Killoran, M.A. Sowole, M.A. Halim, L. Konermann, W.-Y. Choy, Conformational characterization of the intrinsically disordered protein Chibby: Interplay between structural elements in target recognition, Protein Science, 25 (2016) 1420-1429.
[24] S. Zhu, A. Shala, A. Bezginov, A. Sljoka, G. Audette, D.J. Wilson, Hyperphosphorylation of intrinsically disordered tau protein induces an amyloidogenic shift in its conformational ensemble, PLoS One, 10 (2015) e0120416.
[25] C. Lento, S. Zhu, K.A. Brown, R. Knox, P. Liuni, D.J. Wilson, Time-resolved ElectroSpray Ionization Hydrogen-deuterium Exchange Mass Spectrometry for Studying Protein Structure and Dynamics, J Vis Exp, (2017).
[26] E.I. James, T.A. Murphree, C. Vorauer, J.R. Engen, M. Guttman, Advances in Hydrogen/Deuterium Exchange Mass Spectrometry and the Pursuit of Challenging Biological Systems, Chemical Reviews, 122 (2022) 7562-7623.
[27] A. Tischer, M.A. Brehm, V.R. Machha, L. Moon-Tasson, L.M. Benson, K.J. Nelton, R.R. Leger, T. Obser, M. Martinez-Vargas, S.T. Whitten, D. Chen, R.K. Pruthi, H.R. Bergen, M.A. Cruz, R. Schneppenheim, M. Auton, Evidence for the Misfolding of the Al Domain within Multimeric von Willebrand Factor in Type 2 von Willebrand Disease, Journal of Molecular Biology, 432 (2020) 305-323.
[28] D. Smets, A. Tsirigotaki, J.H. Smit, S. Krishnamurthy, A.G. Portaliou, A. Vorobieva, W. Vranken, S. Karamanou, A. Economou, Evolutionary adaptation of the protein folding pathway for secretability, Embo Journal, 41 (2022).
[29] S. Puri, C.Y. Liu, I.C. Hu, C.H. Lai, S.T.D. Hsu, P.C. Lyu, Elucidation of the folding pathway of a circular permutant of topologically knotted YbeA by tryptophan substitutions, Biochemical and Biophysical Research Communications, 672 (2023) 81-88.
[30] W. Hu, Z.Y. Kan, L. Mayne, S.W. Englander, Cytochrome c folds through foldon-dependent native-like intermediates in an ordered pathway, Proc Natl Acad Sci U S A, 113 (2016) 3809-3814.
[31] C. Lento, D.J. Wilson, Subsecond Time-Resolved Mass Spectrometry in Dynamic Structural Biology, Chemical Reviews, 122 (2022) 7624-7646.
[32] Z. Zhang, R.W. Vachet, Kinetics of Protein Complex Dissociation Studied by Hydrogen/Deuterium Exchange and Mass Spectrometry, Anal Chem, 87 (2015) 11777-11783.
[33] J.Y. Zhou, L.Y. Yang, O. Ozohanics, X. Zhang, J.J. Wang, A. Ambrus, P. Arjunan, R. Brukh, N.S. Nemeria, W. Furey, F. Jordan, A multipronged approach unravels unprecedented protein-protein interactions in the human 2-oxoglutarate dehydrogenase multienzyme complex, Journal of Biological Chemistry, 293 (2018) 19213-19227.
[34] K.M. Ramsey, D. Narang, E.A. Komives, Prediction of the presence of a seventh ankyrin repeat in IB epsilon from homology modeling combined with hydrogen-deuterium exchange mass spectrometry (HDX-MS), Protein Science, 27 (2018) 1624-1635.
[35] M.M. Zhang, B.R. Beno, R.Y.C. Huang, J. Adhikari, E.G. Deyanova, J. Li, G.D. Chen, M.L. Gross, An Integrated Approach for Determining a Protein-Protein Binding Interface in Solution and an Evaluation of

Hydrogen-Deuterium Exchange Kinetics for Adjudicating Candidate Docking Models, Analytical Chemistry, 91 (2019) 15709-15717.
[36] A.R. Gutgsell, S.V. Ghodge, A.A. Bowers, S.B. Neher, Mapping the sites of the lipoprotein lipase (LPL)-angiopoietin-like protein 4 (ANGPTL4) interaction provides mechanistic insight into LPL inhibition, Journal of Biological Chemistry, 294 (2019) 2678-2689.
[37] N. Sharma, M.K. Thompson, J.F. Arrington, D.M. Terry, S. Chakravarthy, P.E. Prevelige, A. Prakash, Novel interaction interfaces mediate the interaction between the NEIL1 DNA glycosylase and mitochondrial transcription factor A, Frontiers in Cell and Developmental Biology, 10 (2022).
[38] E. Wolf, C. Lento, J.Y. Pu, B.C. Dickinson, D.J. Wilson, Innate Conformational Dynamics Drive Binding Specificity in Anti-Apoptotic Proteins Mcl-1 and Bcl-2, Biochemistry, 62 (2023) 1619-1630.
[39] S.J. Eron, H.W. Huang, R.V. Agafonov, M.E. Fitzgerald, J. Patel, R.E. Michael, T.D. Lee, A.A. Hart, J. Shaulsky, C.G. Nasveschuk, A.J. Phillips, S.L. Fisher, A. Good, Structural Characterization of Degrader-Induced Ternary Complexes Using Hydrogen-Deuterium Exchange Mass Spectrometry and Computational Modeling: Implications for Structure-Based Design, Acs Chemical Biology, 16 (2021) 2228-2243.
[40] D. Ball, T. Nguyen, N. Zhang, S. D'Arcy, Using hydrogen-deuterium exchange mass spectrometry to characterize Mtr4 interactions with RNA, Methods Enzymol, 673 (2022) 475-516.
[41] T.Y. Liu, P. Limpikirati, R.W. Vachet, Synergistic Structural Information from Covalent Labeling and Hydrogen-Deuterium Exchange Mass Spectrometry for Protein Ligand Interactions, Analytical Chemistry, 91 (2019) 15248-15254.
[42] K.A.T. Makepeace, N.I. Brodie, K.I. Popov, G. Gudavicius, C.J. Nelson, E.V. Petrotchenko, N.V. Dokholyan, C.H. Borchers, Ligand-induced disorder-to-order transitions characterized by structural proteomics and molecular dynamics simulations, Journal of Proteomics, 211 (2020).
[43] S. Tuske, J. Zheng, E.D. Olson, F.X. Ruiz, B.D. Pascal, A. Hoang, J.D. Bauman, K. Das, J.J. DeStefano, K. Musier-Forsyth, P.R. Griffin, E. Arnold, Integrative structural biology studies of HIV-1 reverse transcriptase binding to a high-affinity DNA aptamer, Current Research in Structural Biology, 2 (2020) 116-129.
[44] S.H. Gao, W.J. Zhang, S.L. Barrow, A.T. Iavarone, J.P. Klinman, Temperature-dependent hydrogen deuterium exchange shows impact of analog binding on adenosine deaminase flexibility but not embedded thermal networks, Journal of Biological Chemistry, 298 (2022).
[45] M.L. Fang, O.L.V. Wu, K.A. Cupp-Sutton, K. Smith, S. Wu, Elucidating Protein-Ligand Interactions in Cell Lysates Using High- Throughput Hydrogen-Deuterium Exchange Mass Spectrometry with Integrated Protein Thermal Depletion, Analytical Chemistry, 95 (2023) 1805-1810.
[46] A. Glasgow, H.T. Hobbs, Z.R. Perry, M.L. Wells, S. Marqusee, T. Kortemme, Ligand-specific changes in conformational flexibility mediate long-range allostery in the lac repressor, Nature Communications, 14 (2023).
[47] R.Y. Jia, R.T. Bradshaw, V. Calvaresi, A. Politis, Integrating Hydrogen Deuterium Exchange-Mass Spectrometry with Molecular Simulations Enables Quantification of the Conformational Populations of the Sugar Transporter XylE, Journal of the American Chemical Society, 145 (2023) 7768-7779.
[48] O. Olaleye, C. Graf, B. Spanov, N. Govorukhina, M.R. Groves, N.C. van de Merbel, R. Bischoff, Determination of Binding Sites on Trastuzumab and Pertuzumab to Selective Affimers Using Hydrogen-Deuterium Exchange Mass Spectrometry, Journal of the American Society for Mass Spectrometry, 34 (2023) 775-783.
[49] L. Paco, J.C. Hackett, W.M. Atkins, Nanodisc-embedded cytochrome P450 P3A4 binds diverse ligands by distributing conformational dynamics to its flexible elements, Journal of Inorganic Biochemistry, 244 (2023).
[50] K.M. Burns, M. Rey, C.A.H. Baker, D.C. Schriemer, Platform Dependencies in Bottom-up Hydrogen/Deuterium Exchange Mass Spectrometry*, Molecular & Cellular Proteomics, 12 (2013) 539-548.

[51] O. Ozohanics, A. Ambrus, Hydrogen-Deuterium Exchange Mass Spectrometry: A Novel Structural Biology Approach to Structure, Dynamics and Interactions of Proteins and Their Complexes, Life, 10 (2020) 286.
[52] Z. Zhang, D.L. Smith, Determination of amide hydrogen exchange by mass spectrometry: a new tool for protein structure elucidation, Protein Sci, 2 (1993) 522-531.
[53] K.A. Brown, D.J. Wilson, Bottom-up hydrogen deuterium exchange mass spectrometry: data analysis and interpretation, Analyst, 142 (2017) 2874-2886.
[54] R.S. Johnson, K.A. Walsh, Mass spectrometric measurement of protein amide hydrogen exchange rates of apo- and holo-myoglobin, Protein Sci, 3 (1994) 2411-2418.
[55] R.J. Anderegg, D.S. Wagner, C.L. Stevenson, R.T. Borchardt, The mass spectrometry of helical unfolding in peptides, J Am Soc Mass Spectrom, 5 (1994) 425-433.
[56] J. Pan, J. Han, C.H. Borchers, L. Konermann, Hydrogen/Deuterium Exchange Mass Spectrometry with Top-Down Electron Capture Dissociation for Characterizing Structural Transitions of a 17 kDa Protein, Journal of the American Chemical Society, 131 (2009) 12801-12808.
[57] M. Zehl, K.D. Rand, O.N. Jensen, T.J.D. Jorgensen, Electron Transfer Dissociation Facilitates the Measurement of Deuterium Incorporation into Selectively Labeled Peptides with Single Residue Resolution, Journal of the American Chemical Society, 130 (2008) 17453-17459.
[58] K.D. Rand, C.M. Adams, R.A. Zubarev, T.J.D. Jørgensen, Electron Capture Dissociation Proceeds with a Low Degree of Intramolecular Migration of Peptide Amide Hydrogens, Journal of the American Chemical Society, 130 (2008) 1341-1349.
[59] R.R. Abzalimov, D.A. Kaplan, M.L. Easterling, I.A. Kaltashov, Protein conformations can be probed in top-down HDX MS experiments utilizing electron transfer dissociation of protein ions without hydrogen scrambling, Journal of the American Society for Mass Spectrometry, 20 (2009) 1514-1517.
[60] G.C. Donohoe, J.R. Arndt, S.J. Valentine, Online Deuterium Hydrogen Exchange and Protein Digestion Coupled with Ion Mobility Spectrometry and Tandem Mass Spectrometry, Analytical Chemistry, 87 (2015) 5247-5254.
[61] T.E. Wales, J.R. Engen, Hydrogen exchange mass spectrometry for the analysis of protein dynamics, Mass Spectrom Rev, 25 (2006) 158-170.
[62] L. Konermann, D.A. Simmons, Protein-folding kinetics and mechanisms studied by pulse-labeling and mass spectrometry, Mass Spectrom Rev, 22 (2003) 1-26.
[63] D. Resetca, D.J. Wilson, Characterizing rapid, activity-linked conformational transitions in proteins via sub-second hydrogen deuterium exchange mass spectrometry, Febs j, 280 (2013) 5616-5625.
[64] J.X. Pan, J. Han, C.H. Borchers, L. Konermann, Characterizing Short-Lived Protein Folding Intermediates by Top-Down Hydrogen Exchange Mass Spectrometry, Analytical Chemistry, 82 (2010) 8591-8597.
[65] M. Kish, V. Smith, N. Lethbridge, L. Cole, N.J. Bond, J.J. Phillips, Online Fully Automated System for Hydrogen/Deuterium-Exchange Mass Spectrometry with Millisecond Time Resolution, Analytical Chemistry, (2023).
[66] E. Largy, V. Gabelica, Native Hydrogen/Deuterium Exchange Mass Spectrometry of Structured DNA Oligonucleotides, Analytical Chemistry, 92 (2020) 4402-4410.
[67] E. Largy, A. König, A. Ghosh, D. Ghosh, S. Benabou, F. Rosu, V. Gabelica, Mass Spectrometry of Nucleic Acid Noncovalent Complexes, Chemical Reviews, 122 (2022) 7720-7839.
[68] O.T. Liyanage, M.R. Brantley, E.I. Calixte, T. Solouki, K.L. Shuford, E.S. Gallagher, Characterization of Electrospray Ionization (ESI) Parameters on In-ESI Hydrogen/Deuterium Exchange of Carbohydrate-Metal Ion Adducts, Journal of the American Society for Mass Spectrometry, 30 (2019) 235-247.
[69] N. Sanguantrakun, C. Chanthamontri, M.L. Gross, Top-Down Analysis of In-Source HDX of Native Protein Ions, Journal of the American Society for Mass Spectrometry, 31 (2020) 1151-1154.

[70] E.T. Jansson, Y.H. Lai, J.G. Santiago, R.N. Zare, Rapid Hydrogen-Deuterium Exchange in Liquid Droplets, Journal of the American Chemical Society, 139 (2017) 6851-6854.
[71] X. Li, K. Attanayake, S.J. Valentine, P. Li, Vibrating Sharp-edge Spray Ionization (VSSI) for voltage-free direct analysis of samples using mass spectrometry, Rapid Communications in Mass Spectrometry, 35 (2021).
[72] C. Li, K. Attanayake, S.J. Valentine, P. Li, Facile Improvement of Negative Ion Mode Electrospray Ionization Using Capillary Vibrating Sharp-Edge Spray Ionization, Analytical Chemistry, 92 (2020) 2492-2502.
[73] A. DeBastiani, S.N. Majuta, D. Sharif, K. Attanayake, C. Li, P. Li, S.J. Valentine, Characterizing Multidevice Capillary Vibrating Sharp-Edge Spray Ionization for In-Droplet Hydrogen/Deuterium Exchange to Enhance Compound Identification, ACS Omega, 6 (2021) 18370-18382.
[74] S.N. Majuta, C. Li, K. Jayasundara, A.K. Karanji, K. Attanayake, N. Ranganathan, P. Li, S.J. Valentine, Rapid Solution-Phase Hydrogen/Deuterium Exchange for Metabolite Compound Identification, Journal of the American Society for Mass Spectrometry, 30 (2019) 1102-1114.
[75] D.R. Sharif, M.; Mahmud, S.; Sultana, M. N.; Attanayake, K.; DeBastiani, A.; Foroushani, S. H.; Li, P.; Valentine, S. J., In-droplet hydrogen-deuterium exchange (HDX) to examine protein/peptide solution conformer heterogeneity, Rapid Communications in Mass Spectrometry, (in press) (2023).
[76] M. Girod, E. Moyano, D.I. Campbell, R.G. Cooks, Accelerated bimolecular reactions in microdroplets studied by desorption electrospray ionization mass spectrometry, Chemical Science, 2 (2011) 501-510.
[77] A.K. Badu-Tawiah, D.I. Campbell, R.G. Cooks, Accelerated C-N Bond Formation in Dropcast Thin Films on Ambient Surfaces, Journal of the American Society for Mass Spectrometry, 23 (2012) 1461-1468.
[78] T. Muller, A. Badu-Tawiah, R.G. Cooks, Accelerated Carbon-Carbon Bond-Forming Reactions in Preparative Electrospray, Angewandte Chemie-International Edition, 51 (2012) 11832-11835.
[79] J.K. Lee, S. Banerjee, H.G. Nam, R.N. Zare, Acceleration of reaction in charged microdroplets, Q Rev Biophys, 48 (2015) 437-444.
[80] A. Fallah-Araghi, K. Meguellati, J.-C. Baret, A.E. Harrak, T. Mangeat, M. Karplus, S. Ladame, C.M. Marques, A.D. Griffiths, Enhanced Chemical Synthesis at Soft Interfaces: A Universal Reaction-Adsorption Mechanism in Microcompartments, Physical Review Letters, 112 (2014) 028301.
[81] C.J. Chen, E.R. Williams, The role of analyte concentration in accelerated reaction rates in evaporating droplets, Chemical Science, 14 (2023) 4704-4713.
[82] S. Burge, G.N. Parkinson, P. Hazel, A.K. Todd, S. Neidle, Quadruplex DNA: sequence, topology and structure, Nucleic Acids Res, 34 (2006) 5402-5415.
[83] A. Ghosh, E. Largy, V. Gabelica, DNA G-quadruplexes for native mass spectrometry in potassium: a database of validated structures in electrospray-compatible conditions, Nucleic Acids Res, 49 (2021) 2333-2345.
[84] A. Marchand, V. Gabelica, Folding and misfolding pathways of G-quadruplex DNA, Nucleic Acids Research, 44 (2016) 10999-11012.
[85] S. Kingdom, Multiple Linear Regression Calculator, in, Melbourne, Australia, 2017.
[86] D. Sen, W. Gilbert, Formation of parallel four-stranded complexes by guanine-rich motifs in DNA and its implications for meiosis, Nature, 334 (1988) 364-366.
[87] C.D. Xiao, T. Ishizuka, Y. Xu, Antiparallel RNA G-quadruplex Formed by Human Telomere RNA Containing 8-Bromoguanosine, Sci Rep, 7 (2017) 6695.
[88] A.T. Phan, J.L. Mergny, Human telomeric DNA: G-quadruplex, i-motif and Watson-Crick double helix, Nucleic Acids Res, 30 (2002) 4618-4625.
[89] A.T. Phan, Human telomeric G-quadruplex: structures of DNA and RNA sequences, FEBS J, 277 (2010) 1107-1117.

[90] J.A. Capra, K. Paeschke, M. Singh, V.A. Zakian, G-quadruplex DNA sequences are evolutionarily conserved and associated with distinct genomic features in Saccharomyces cerevisiae, PLoS Comput Biol, 6 (2010) e1000861.
[91] Y. Wang, D.J. Patel, Solution structure of the human telomeric repeat d[AG3(T2AG3)3] G-tetraplex, Structure, 1 (1993) 263-282.
[92] S. Balasubramanian, S. Neidle, G-quadruplex nucleic acids as therapeutic targets, Curr Opin Chem Biol, 13 (2009) 345-353.
[93] R. Eritja, J.L. Mergny, D. Montesarchio, L. Spindler, M. Webba da Silva, G-quadruplex nucleic acids, J Nucleic Acids, 2010 (2010).
[94] C.J. Lech, B. Heddi, A.T. Phan, Guanine base stacking in G-quadruplex nucleic acids, Nucleic Acids Res, 41 (2013) 2034-2046.
[95] E. Largy, J.L. Mergny, V. Gabelica, Role of Alkali Metal Ions in G-Quadruplex Nucleic Acid Structure and Stability, Met Ions Life Sci, 16 (2016) 203-258.
[96] A. Wong, G. Wu, Selective binding of monovalent cations to the stacking G-quartet structure formed by guanosine 5'-monophosphate: a solid-state NMR study, J Am Chem Soc, 125 (2003) 13895-13905.
[97] M. Webba da Silva, Geometric formalism for DNA quadruplex folding, Chemistry, 13 (2007) 9738-9745.
[98] A. Jain, G. Wang, K.M. Vasquez, DNA triple helices: Biological consequences and therapeutic potential, Biochimie, 90 (2008) 1117-1130.
[99] S. Daly, F. Rosu, V. Gabelica, Mass-resolved electronic circular dichroism ion spectroscopy, Science, 368 (2020) 1465-1468.
[100] D.F. Sharif, S. H.; Attanayake, K.; Dewasurendra, V. K.; DeBastiani, A.; DeVor, A.; Johnson, M. B.; Li, P.; Valentine, S. J., Capillary Vibrating Sharp-Edge Spray Ionization Augments Field-Free Ionization Techniques to Promote Conformer Preservation in the Gas-Phase for Intractable Biomolecular Ions, Journal of Physical Chemistry B, (in press) (2022).
[101] K.N. Luu, A.T. Phan, V. Kuryavyi, L. Lacroix, D.J. Patel, Structure of the Human Telomere in K+Solution: An Intramolecular (3 + 1) G-Quadruplex Scaffold, Journal of the American Chemical Society, 128 (2006) 9963-9970.
[102] J. Dai, M. Carver, C. Punchihewa, R.A. Jones, D. Yang, Structure of the Hybrid-2 type intramolecular human telomeric G-quadruplex in K+ solution: insights into structure polymorphism of the human telomeric sequence, Nucleic Acids Research, 35 (2007) 4927-4940.
[103] H.R. Drew, R.M. Wing, T. Takano, C. Broka, S. Tanaka, K. Itakura, R.E. Dickerson, Structure of a B-DNA dodecamer: conformation and dynamics., Proceedings of the National Academy of Sciences, 78 (1981) 2179-2183.
[104] E. Largy, M. Ranz, OligoR: A Native HDX/MS Data Processing Application Dedicated to Oligonucleotides, Analytical Chemistry, 95 (2023) 9615-9622.
[105] J.B. Fenn, M. Mann, C.K. Meng, S.F. Wong, C.M. Whitehouse, ELECTROSPRAY IONIZATION FOR MASS-SPECTROMETRY OF LARGE BIOMOLECULES, Science, 246 (1989) 64-71.
[106] M. Wilm, M. Mann, Analytical Properties of the Nanoelectrospray Ion Source, Analytical Chemistry, 68 (1996) 1-8.
[107] M.S. Wilm, M. Mann, ELECTROSPRAY AND TAYLOR-CONE THEORY, DOLES BEAM OF MACROMOLECULES AT LAST, International Journal of Mass Spectrometry, 136 (1994) 167-180.
[108] S.-J. Hyung, C.V. Robinson, B.T. Ruotolo, Gas-Phase Unfolding and Disassembly Reveals Stability Differences in Ligand-Bound Multiprotein Complexes, Chemistry & Biology, 16 (2009) 382-390.
[109] J.D. Eschweiler, J.N. Rabuck-Gibbons, Y.W. Tian, B.T. Ruotolo, CIUSuite: A Quantitative Analysis Package for Collision Induced Unfolding Measurements of Gas-Phase Protein Ions, Analytical Chemistry, 87 (2015) 11516-11522.

[110] d. An, A.; Tidwell, E.; Gadkari, V.; Koutmos, M.; Ruotolo B., Collision Induced Unfolding Reveals Disease-Associated Stability Shifts in Mitochondrial tRNAs. , in, ChemRxiv. Cambridge: Cambridge Open Engage; 2023; This content is a preprint and has not been peer-reviewed., 2023.